

Zn对砖块状单斜WO₃光催化活性的影响

肖忠连^{#1} 伍轩逸^{#1} 谭贺云¹ Paolo Aprea² 郝仕油^{*1}

(¹浙江师范大学行知学院, 化学与生命科学学院, 金华 321004)

(²费德里克二世大学, 化学、材料与制造工程系, 那不勒斯 80125, 意大利)

摘要: 利用简单的方法合成了Zn掺杂砖块状WO₃材料,并用罗丹明B对其光催化性能进行了评估。利用X射线衍射、拉曼光谱、扫描电镜、紫外可见漫反射光谱、红外光谱和X射线光电子能谱分析等技术对合成材料进行了表征,结果表明适量Zn掺杂可保持WO₃的砖块状形貌。光催化结果表明Zn掺杂量(质量分数)为5%的WO₃光催化性能最好,这是因为该材料内形成了大量的氧空位且羟基含量较高。

关键词: 锌; 三氧化钨; 合成; 光催化; 氧空位

中图分类号: O614.24⁺¹; O614.61⁺³

文献标识码: A

文章编号: 1001-4861(2021)09-1700-07

DOI:10.11862/CJIC.2021.189

Effect of Zn on Photocatalytic Activity of Block-Shaped Monoclinic WO₃

XIAO Zhong-Lian^{#1} WU Xuan-Yi^{#1} TAN He-Yun¹ Paolo Aprea² HAO Shi-You^{*1}

(¹Xingzhi College, College of Chemistry and Life Sciences, Zhejiang Normal University, Jinhua, Zhejiang 321004, China)

(²Department of Chemical, Materials and Production Engineering, University Federico II, Naples 80125, Italy)

Abstract: Zn-doped block-shaped monoclinic WO₃ composite (Zn-doped WO₃) was synthesized via a facile method and the photocatalytic activity of rhodamine B (RhB) over Zn-doped WO₃ was evaluated. The prepared samples were characterized by X-ray diffraction, Raman spectrum, scanning electron micrograph, UV-Vis diffuse reflection spectrum, Fourier transform infrared spectrum, and X-ray photoelectron spectrum and other techniques, and the results showed that the block-shaped monoclinic WO₃ did not be changed by appropriate amount of Zn doping. The photocatalytic results illustrated that mass ratio of 5% Zn doped WO₃ performed the best photocatalytic efficiency due to the formation of more oxygen vacancy and the increase of hydroxyl groups number.

Keywords: Zn; WO₃; synthesis; photocatalysis; oxygen vacancy

It is well known that the pollution resulting from dye wastewater has become one of the most serious environmental problems due to the wide usage of dyes in textiles, leather, papermaking, food additives, cosmetics, etc^[1]. These dye wastewater may cause direct severe damage to the liver system, digestive system, and human beings because toxic by-products can be pro-

duced from the discharged dyes via oxidation, hydrolysis, and other chemical reactions^[2-3]. Therefore, the wastewater containing dyes must be eliminated before being discharged into the environment. At present, many methods such as physical adsorption^[4], chemical precipitation^[5], and photocatalytic degradation^[6], have been used to remove dyes from wastewater. Among

收稿日期:2021-03-21。收修改稿日期:2021-06-08。

国家自然科学基金项目(No.21876158)资助。

[#]共同第一作者。

^{*}通信联系人。E-mail:sky54@zjnu.cn

these approaches, semiconductor-based photocatalysis is considered as a highly effective technology for the removal of organic dyes because organic pollutants can be degraded into H₂O and CO₂ over the semiconductor photocatalyst. As is reported that WO₃ play an important role in the field of photocatalysis due to its narrow band gap of about 2.8 eV^[7] and hence potentially efficient visible light absorbance. Generally, WO₃ possesses monoclinic, triclinic, orthogonal or hexagonal crystal structure at different temperatures^[8]. It can be concluded that monoclinic WO₃ has efficiently photocatalytic performance because of its lowest band gap (about 2.65 eV at room temperature^[9]). Recently, we found that the photocatalytic efficiency of monoclinic WO₃ was greatly affected by its morphology, and a block-shaped morphology was beneficial for the improvement of its photocatalysis^[10]. However, the photocatalytic activity of pure WO₃ is not satisfactory because of its inherent defects such as relatively low conduction-band level^[11]. In order to improve the photocatalytic efficiency of WO₃, doping with metal and nonmetal elements is often used to form WO₃ based composite structure such as WO₃/TiO₂^[12], WO₃/CuO^[13], and WO₃/C₃N₄^[14]. As a promising alternative semiconductor, ZnO has attracted wide attention in the field of photocatalysis^[15-17] because of potentially photocatalytic activity, low-cost and environmentally friendly feature. Because of the similar ionic radius of Zn²⁺ to that of W⁶⁺, it can be concluded that Zn²⁺ may penetrate into the WO₃ crystal lattice or substitute the W⁶⁺ position in the crystal, resulting in easy generation of lattice defects and hence improvement of WO₃ photocatalysis. Recently, Zn doped WO₃ with different morphologies such as spherical, rod shaped or nanoporous morphology were synthesized and the photocatalytic activity of the resulted samples was also investigated^[18-19]. However, to the best of our knowledge, there have no study investigating the photocatalytic property of Zn doped monoclinic WO₃ with a block-shaped morphology.

Herein, Zn doped block-shaped monoclinic WO₃ was prepared via a facile method and the photocatalytic degradation of rhodamine (RhB) was carried out. The photocatalytic results show that appropriate amount of

Zn doping can improve the photocatalytic activity of block-shaped monoclinic WO₃ due to the formation of oxygen vacancy and the increase of hydroxyl groups number.

1 Experimental

1.1 Materials synthesis

Na₂WO₄·2H₂O, Zn(NO₃)₂·6H₂O, polyvinylpyrrolidone (PVP), absolute ethanol, sodium hydroxide (NaOH), 37% fuming hydrochloric acid (concentrated HCl), RhB, terephthalic acid (TPA), 1,4-benzoquinone (BQ) and KI were purchased from Sinopharm Chemical Reagent Co. All the chemical reagents were used without further purification. Deionized water, with a resistivity larger than 18.2 MΩ, was obtained from Millipore Milli-Q[®] ultrapure water purification systems and used to prepare 0.1 mol·L⁻¹ HCl and 0.1 mol·L⁻¹ NaOH solutions (diluting the fuming hydrochloric acid and dissolving solid NaOH, respectively).

Typically, solution A was prepared by dissolving 4 g of PVP in 10 mL H₂O at room temperature under stirring for 10 min, by adding 10 mL of concentrated HCl, and then by aging the solution for 60 min. Similarly, solution B was prepared by dissolving 3.3 g of Na₂WO₄·2H₂O in 10 mL H₂O at room temperature. Afterwards, solution B was slowly added to solution A under stirring for 30 min to form a yellow precipitate (H₂WO₄). The mixed solution was stirred for another 30 min, transferred into a Teflon autoclave, and the synthesis was carried out without agitation in oven at 180 °C for 12 h. The product was filtered and the solid was washed three times with deionized water, followed by washing for another three times with absolute ethanol. The washed solid was then dried at 60 °C overnight and a pale-yellow pre-product (a mixture of H₂WO₄ and WO₃) was obtained.

A typical synthesis of Zn(OH)₂ was performed as follows: at room temperature, 1 g of Zn(NO₃)₂·6H₂O was added to 60 mL H₂O under stirring for 30 min, and then 2 mol·L⁻¹ NaOH was added dropwise until no formation of white precipitant. Afterwards, Zn(OH)₂ was obtained by filtration, washed for 3 times with water and ethanol, respectively, and then dried at 60 °C.

Zn-doped WO_3 was synthesized by the following procedure. 0.5 g of the resulted mixture of H_2WO_4 and WO_3 and x g ($x=0.015, 0.025, 0.035$) of $\text{Zn}(\text{OH})_2$ placed in the agate mortar were grinded for 30 min, and then calcined at $550\text{ }^\circ\text{C}$ for 2 h. Finally, different amounts of Zn doped WO_3 samples were obtained, and the samples were denoted as 3%Zn- WO_3 , 5%Zn- WO_3 , and 7%Zn- WO_3 , respectively. For comparison purposes, WO_3 was synthesized under the same experimental conditions, except that no $\text{Zn}(\text{OH})_2$ was added.

1.2 Characterization

The X-ray diffraction (XRD) patterns were collected on a Philips PW3040/60 powder diffractometer using Cu $K\alpha$ radiation ($\lambda=0.154\text{ nm}$). The X-ray tube was operated at 40 kV and 40 mA, and scanning interval ranged from 10° to 80° . Raman scattering analysis was performed on a Renishaw RM1000 Raman spectrometer with a 514 nm excitation laser light. Scanning electron microscope (SEM) images were obtained using a Hitachi S-4800 instrument under an accelerating voltage of 20~40 kV, 0.2~5 kV in 100 V steps, and 5~40 kV in 1 kV steps. The UV-Vis diffuse reflectance (DRS) spectra of the samples over a range of 200~1 000 nm were recorded by a Nicolet Evolution 500 Scan UV-Vis system with a scanning rate of $60\text{ nm}\cdot\text{min}^{-1}$. The FT-IR spectra were recorded by a Nicolet Nexus 670 spectrometer with a resolution of 4 cm^{-1} using KBr pellet method. The photoluminescence (PL) spectra of the samples were obtained at room temperature by a spectrofluorometer (NanoLOG-TCSPC, Horiba Jobin Yvon, USA) with an excitation wavelength of 325 nm. X-ray photoelectron spectroscopy (XPS) measurement was carried out on a RBO upgraded PHI-5000 C ESCA system (Perkin Elmer) using monochromated Al $K\alpha$ X-rays ($E=1486.6\text{ eV}$) as a radiation at 250 W operating at an accelerating voltage of 15 kV. All binding energies were calibrated using carbon (C1s, 284.6 eV) as a reference.

1.3 Photocatalytic tests

The photocatalytic activities of WO_3 , 3%Zn- WO_3 , 5%Zn- WO_3 , and 7%Zn- WO_3 were evaluated by the photodegradation of RhB under visible light irradiation. In a typical experiment, 50 mg of photocatalyst

(WO_3 , 3%Zn- WO_3 , 5%Zn- WO_3 or 7%Zn- WO_3) was dispersed into 50 mL of RhB solution ($5\text{ mg}\cdot\text{L}^{-1}$) under magnetic stirring for 15 min. The pH of all the solutions containing RhB used for the photocatalytic experiments was adjusted to the desired value using $0.1\text{ mol}\cdot\text{L}^{-1}$ HCl and/or NaOH solutions. Afterwards, the suspensions were stirred in the dark for 30 min to reach the equilibrium. At given time intervals, a small amount of suspension was withdrawn and centrifuged to remove the photocatalyst. The residual RhB levels in the filtrates were then analyzed by recording the variations of the absorbance at 552 nm with a UV-Vis spectrophotometer (Evolution 500LC). The removal efficiency of RhB was evaluated as η :

$$\eta=(A_0-A)/A_0\times 100\% \quad (1)$$

Where A_0 is the initial absorbance of RhB and A is the absorbance of RhB in the filtrates.

2 Results and discussion

The crystalline structure of WO_3 and the samples prepared with different Zn amounts were characterized by XRD technique, which is presented in Fig. 1a. It can be seen from Fig. 1a that the XRD patterns of all the samples can be identified as monoclinic WO_3 (PDF No.46-1096), whose characteristic peaks are located at $23.1^\circ, 23.6^\circ, 24.4^\circ, 33.3^\circ, 34.2^\circ$ which corresponding to (002), (020), (200), (120), (202)^[20]. It is obvious from Fig. 1a that the characteristic peak located at about 30.68° (marked with five pointed star) can be detected for the Zn-doped samples, which is the (100) reflection of ZnO. It also can be found from Fig. 1a that the intensity of (100) reflection increased with the increasing of Zn doping amount, implying that Zn can effectively entry into WO_3 lattice, in good agreement with our above inference. The Raman spectra of as-prepared Zn-doped WO_3 were also recorded and compared with that of WO_3 in the range of 200~1 000 cm^{-1} (Fig. 1b). The peaks at around 270.4, 715.8 and 805.8 cm^{-1} are typical features of the monoclinic structure of WO_3 ^[21], which is consistent with the XRD results. The lack of the peak at approximately 950 cm^{-1} attributed to the stretching mode of $\text{W}^{6+}=\text{O}$ ^[22], confirms the crystallinity of the catalysts. After Zn doping, the two most

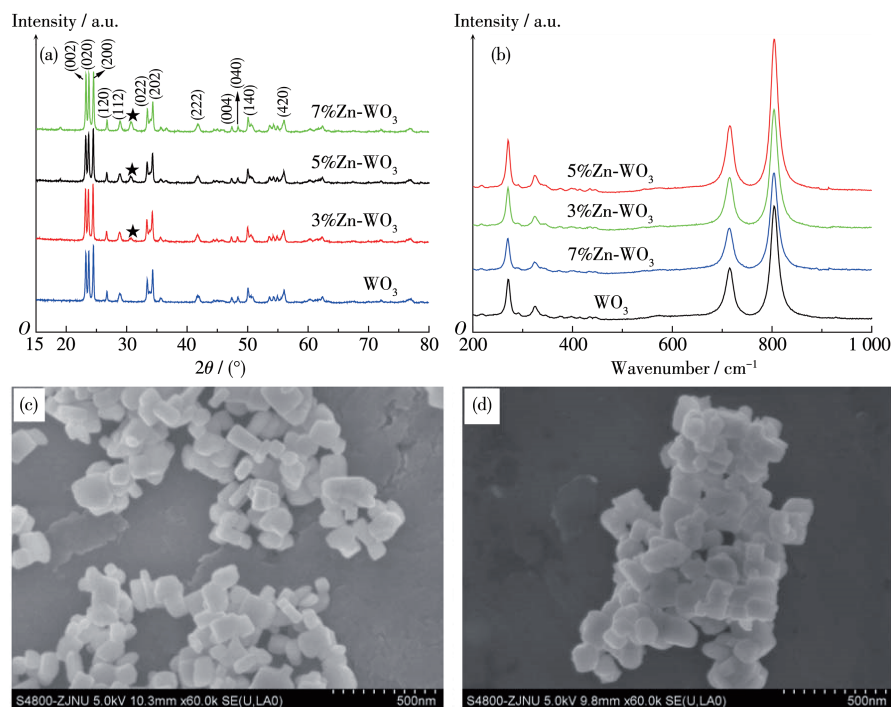


Fig.1 XRD patterns (a) and Raman spectra (b) of WO₃, 3%Zn-WO₃, 5%Zn-WO₃, and 7%Zn-WO₃; SEM images of WO₃ (c) and 5%Zn-WO₃ (d)

intense peaks at 715.8 and 805.8 cm⁻¹, corresponding to O—W—O vibration mode, became wider. Furthermore, the Raman band at about 325 cm⁻¹ assigned to 2E₂ (M) vibration mode of hexagonal wurtzite ZnO^[23] was observed in Zn doped WO₃ samples, confirming the presence of Zinc in the catalyst. The result (Fig.S1) further prove the presence of Zinc in the synthesized samples. It can be seen from Fig.1c and 1d that WO₃ and 5%Zn-WO₃ have a block-shaped morphology. Other Zn doped samples also have similar structures to that of WO₃, indicating that Zn doping amount arranging from 3% to 7% can not change the block-shaped morphology of initial WO₃.

The photocatalytic activities of WO₃, 3%Zn-WO₃, 5%Zn-WO₃, and 7%Zn-WO₃ are showed in Fig.2. It is clear that the photocatalytic efficiency of WO₃ increased when Zn doping amount increased from 3% to 5%, but decreased when the doping amount exceeded 5%. Fig.3 can explain the above experimental results. The photocatalytic results show that an appropriate amount of Zn doping is good for the improvement of WO₃ photocatalysis performance. It can be concluded from Fig.S2 that RhB was actually degraded over 5%Zn-WO₃.

In order to explain the above photocatalytic results, UV - Vis DRS and PL spectra of WO₃, 3%Zn-WO₃, 5%Zn-WO₃, and 7%Zn-WO₃ were recorded and the results are shown in Fig.3. It can be seen from Fig.3a that the light (especially visible light) absorption efficiency of 5%Zn-WO₃ was higher than that of WO₃, resulting in efficient generation of photogenerated electrons and holes over 5%Zn-WO₃ under the irradiation of visible light. The PL spectra of pure WO₃ and Zn

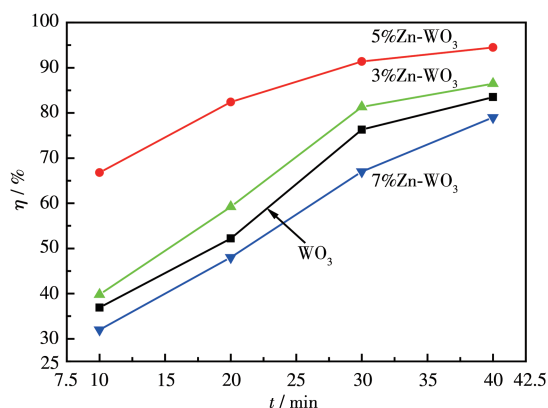
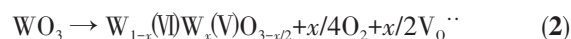


Fig.2 Photodegradation of 5 mg·L⁻¹ RhB in the presence of different photocatalysts under visible light irradiation at pH of 6 ($V_{\text{RhB}}=50$ mL, $m_{\text{photocatalyst}}=0.05$ g)

doped WO_3 are shown in Fig.3b. It is obvious that the position and pattern of the emission peaks of all samples were almost similar, but the PL intensities of the samples were noticeably different. Generally, the lower the PL intensity, the higher the separation efficiency for photogenerated electron-hole pairs^[24]. From Fig.3b, it is easy to find that the PL intensity of 5%Zn- WO_3 was the lowest, indicating that the charge separation efficient in 5%Zn- WO_3 was better than that in WO_3 . This may be due to the fact that the photogenerated electrons and holes are separated by the charge transfer at the heterojunction interfaces of 5%Zn- WO_3 . Consequently, the photocatalytic activity of 5%Zn- WO_3 was higher than that of WO_3 . It can be seen that the light absorption efficiency of 7%Zn- WO_3 was lower than those of other samples, and the PL intensity of it was the highest one, resulting in the lowest photocatalytic activity.

In order to study the reason why 5%Zn- WO_3 had higher separation efficiency of photogenerated electron-hole pairs, W4f XPS spectra for 5%Zn- WO_3 and WO_3 were carried out (Fig.4). It is clear from Fig.4 that the

W4f_{7/2} and W4f_{5/2} peaks centered at 35.4 and 37.6 eV are typical binding energies corresponding to W⁶⁺ oxidation state^[25]. Moreover, the peak at about 36.2 eV corresponding to orbital spin of W⁵⁺4f_{5/2}^[26] was detected in 5%Zn- WO_3 and WO_3 , but the peak intensity of the former was higher than that of the latter, implying that Zn doping is beneficial for the formation of W⁵⁺. The possible reason is that Zn²⁺ is beneficial to the interaction between WO_3 precursor (H_2WO_4) and PVP. Therefore, the W⁶⁺ is easier to be reduced by PVP in 5%Zn- WO_3 precursor than in the WO_3 precursor, resulting in a larger number of oxygen vacancies arising from the replacement of W⁶⁺ by W⁵⁺ in 5%Zn- WO_3 , as expressed by the following equation:



Where $\text{V}_0^{\cdot\cdot}$ represents an oxygen vacancy. From our previous report^[27], it can be concluded that the photogenerated electrons can be easily captured by oxygen vacancy, which can cause efficient separation efficiency for photogenerated electron-hole pairs. Therefore, the photocatalytic efficiency of 5%Zn- WO_3 was higher than that of WO_3 .

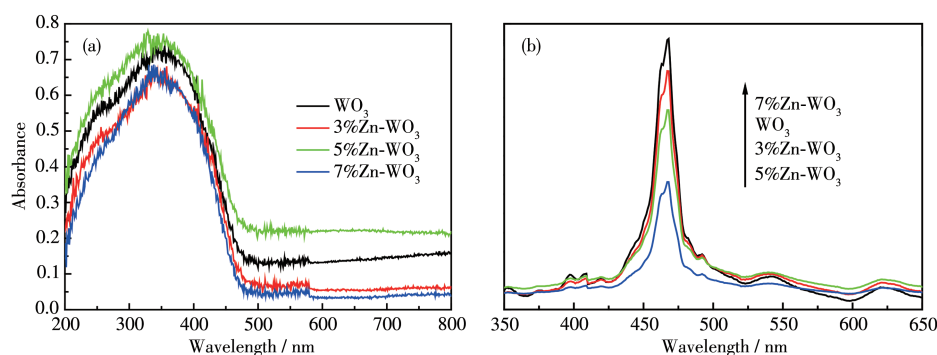


Fig.3 UV-Vis DRS (a) and PL (b) spectra of WO_3 , 3%Zn- WO_3 , 5%Zn- WO_3 , and 7%Zn- WO_3

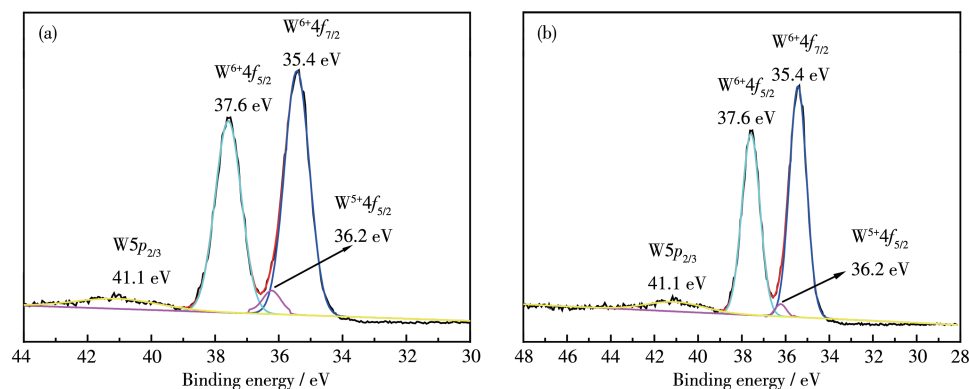


Fig.4 W4f XPS spectra for 5%Zn- WO_3 (a) and WO_3 (b)

Besides the above factor affecting the photocatalytic activity, the adsorption ability of dyes on the surface of photocatalyst also play an important role. It is reported that the content of hydroxyl groups on the surface of photocatalyst can greatly influence the adsorption ability of RhB and hence the photocatalytic efficiency^[28]. Generally, the content of hydroxyl groups can be reflected by the O1s XPS spectra^[29]. In order to invest the effect of Zn doping on the content of hydroxyl groups on the surface of WO₃, the O1s XPS spectra of 5%Zn-WO₃ and WO₃ were obtained (Fig.5). According to Han et al., the peak at about 530.5 eV is related to oxygen in the lattice (O²⁻, O II), and another peak, located at about 531.5 eV, corresponds to adsorbed oxygen (O I) in the form of O—H on the surface^[30]. Generally, the content of hydroxyl groups can be

reflected by the ratio of S_{O I} (the peak area of adsorbed oxygen in the form of O—H) to S_{O II} (the peak area of oxygen in the lattice). The higher the value of S_{O I}/S_{O II}, the richer the content of hydroxyl groups in the prepared sample. It can be found from Fig.5 that the value of S_{O I}/S_{O II} for 5%Zn-WO₃ was higher than that for WO₃, implying that the content of hydroxyl groups in 5%Zn-WO₃ was higher than that in WO₃. The reason may be that Zn²⁺ is easy to combined with OH⁻ to form [Zn(OH)₄]²⁻ coordination ion, which is good for the improvement of hydroxyl content in the precursor of 5%Zn-WO₃. Consequently, the adsorbed amount of RhB on 5%Zn-WO₃ was higher than that on WO₃, resulting in a higher photocatalytic activity. The results of Fig.S3 show that •O₂⁻ and h⁺ are the main active species to degrade RhB.

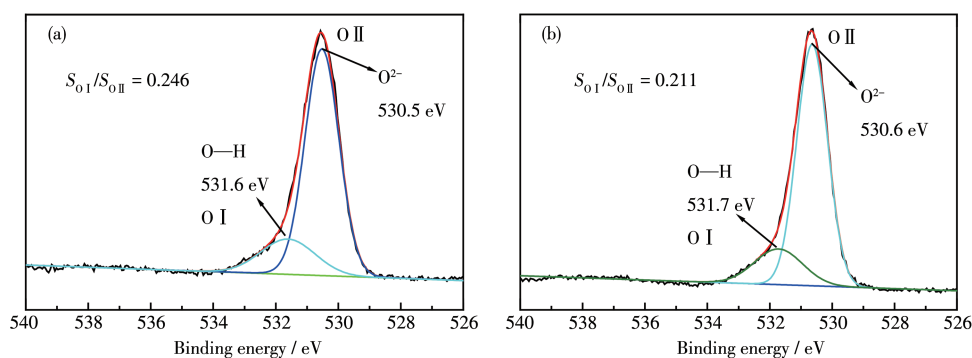


Fig.5 O1s XPS spectra for 5%Zn-WO₃ (a) and WO₃ (b)

3 Conclusions

In summary, Zn-doped WO₃ was synthesized by a facile method. The photocatalytic results show that the photocatalytic activity of WO₃ is enhanced after doping of Zn because the photoelectrons and holes can be efficiently separated due to the formation of oxygen vacancies. Furthermore, Zn doping can improve the content of hydroxyl groups, which is beneficial for the improvement of RhB adsorption ability and hence the photocatalytic efficiency.

Acknowledgement: This work was supported by the National Natural Science Foundation of China (Grant No.21876158).

Supporting information is available at <http://www.wjhxxb.cn>

References:

- [1] Kim K H, Ihm S K. *J. Hazard. Mater.*, **2011**,**186**:16-34
- [2] Liu X D, Yan L, Yin W Y, Zhou L J, Tian G, Shi J X, Yang Z Y, Xiao D B, Gu Z J, Zhao Y L. *J. Mater. Chem. A*, **2014**,**2**:12296-12303
- [3] Salleh M A M, Mahmoud D K, Karim W A, Idris A. *Desalination*, **2011**,**280**:1-13
- [4] Koyuncu, D D E, Okur M. *Sep. Purif. Technol.*, **2021**,**257**:117657
- [5] Liu Y, Xu D L, Wang P, Dong Y H. *Desalin. Water Treat.*, **2016**,**57**: 6772-6780
- [6] Wang Y F, Geng Q J, Yang J M, Liu, Y, Liu C. *ACS Omega*, **2020**,**5**: 31137-31145
- [7] Malato S, Fernandez-Ibanez P, Maldonado M I, Blanco J, Gernjak W. *Catal. Today*, **2009**,**147**:1-60
- [8] Roussel P, Labbe P, Groult D. *Acta Crystallogr. Sect. B: Struct. Sci.*, **2000**,**56**:377-399
- [9] Gillet M, Aguir K, Lemire C, Gillet E, Schierbaum K. *Thin Solid Films*, **2004**,**467**:239-246

- [10]Shang J, Xiao Z L, Yu L X, Aprea P, Hao S Y. *Nanotechnology*, **2020**,**31**:125603
- [11]Xi G C, Yue B, Cao J Y, Ye J H. *Chem. Eur. J.*, **2011**,**17**:5145-5154
- [12]Odhiambo V O, Ongarbayeva A, Keri O, Simon L, Szilagyi I M. *Nanomaterials*, **2020**,**10**:882
- [13]Dursun S, Koyuncu S N, Kaya I C, Kaya G G, Kalem V, Akyildiz H. *J. Water Process Eng.*, **2020**,**36**:101390
- [14]Truong H B, Huy B T, Ray S K, Lee Y I, Cho J, Hur J. *Chem. Eng. J.*, **2020**,**399**:125733
- [15]Zeng W, Ren Y F, Zheng Y Y, Pan A Q, Zhu T. *ChemCatChem*, **2021**,**13**:564-573
- [16]Lin Y, Hu H Y, Hu Y H. *Appl. Surf. Sci.*, **2020**,**502**:144202
- [17]Chen J, Xiong Y, Duan M, Li X, Li J, Fang S W, Qin S, Zhang R. *Langmuir*, **2020**,**36**:520-533
- [18]Arshad M, Ehtisham - ul - Haque S, Bilal M, Ahmad N, Ahmad A, Abbas M, Nisar J, Khan M I, Nazir A, Ghaffar A, Iqba M. *Mater. Res. Express*, **2020**,**7**:015407
- [19]Santhi K, Rani C, Kumar R D, Karuppuchamy S. *J. Mater. Sci.: Mater. Electron.*, **2015**,**26**:10068-10074
- [20]Chen S H, Xiao Y, Xie W, Wang Y H, Hu Z F, Zhang W, Zhao H. *Nanomaterials*, **2018**,**8**:1-13
- [20]Djaoued Y, Balaji S, Bruning R. *J. Nanomater.*, **2012**,**2012**:674168
- [22]Huang Y S, Zhang Y Z, Zeng X T, Hu X F. *Appl. Surf. Sci.*, **2002**, **202**:104-109
- [23]Akira S, Hamdi A, Addad A, Coffinier Y, Boukherroub R, Omrani A D. *Appl. Surf. Sci.*, **2017**,**400**:461-470
- [24]Samanta S, Martha S, Parida K. *ChemCatChem*, **2014**,**6**:1453-1462
- [25]Annanouch E F, Roso S, Haddi Z, Vallejos S, Umek P, Bittencourt C, Blackman C, Vilic T, Llobe E. *Thin Solid Films*, **2016**,**618**:238-245
- [26]Ozin G A, Prokopowicz R A, Ozkar S. *J. Am. Chem. Soc.*, **1992**,**114**: 8953-8963
- [27]Hao S Y, Hou J, Aprea P, Pepe F. *Appl. Catal. B*, **2014**,**160-161**:566-573
- [28]Hao S Y, Hou J, Aprea P, Lv T X. *Ind. Eng. Chem. Res.*, **2014**,**53**: 14617-14622
- [29]Wang Y G, Li B, Zhang C L, Cui L F, Kang S F, Li X, Zhou L H. *Appl. Catal. B*, **2013**,**130-131**:277-84
- [30]Han H G, Li H P, Fu L, Yang J, Liu Z. *Chem. Phys. Lett.*, **2016**,**651**: 183-187